GEOFIZIKA VOL. 42 2025

DOI: https://doi.org/10.15233/gfz.2025.42.8
Original scientific paper

CC BY NC

Study on the response characteristics of source parameters for strong mining tremors

Shaohui Zhou, Junhao Qu, Shuang Wu and Yu Wang

Shandong Earthquake Agency, Jinan, China

Received 14 February 2025, in final form 18 July 2025

Mine tremors are a significant factor contributing to safety accidents in mining areas, and studying the characteristics of the rupture process at the source of mine tremor is crucial for improving the understanding of the disaster mechanism caused by mine tremors. This paper conducts an in-depth analysis and study of 39 strong mine tremor in Shandong mining areas in China using a combination of numerical simulation and theoretical analysis. Firstly, the waveform recording of strong mine tremors is processed using Fast Fourier Transform (FFT). Subsequently, the noise term, instrument response, path effect, and site response of the monitoring station are eliminated from the waveform recording. Finally, based on the Brune source model, a genetic algorithm is utilized to fit and obtain the source parameters. The response characteristics of source parameters for strong mining tremors are analyzed, and the scale of focal rupture as well as the characteristics of regional stress release are revealed. The results showed that the calculated corner frequencies, seismic moments, moment magnitudes, and stress drops of these strong mining tremors were in the ranges of 0.9–2.6 Hz, 10^{12}–10^{14} N m, 2.5–3.5, and 0.02–0.18 MPa, respectively. The results showed that the mine tremors exhibited cross-correlation relationships between the source parameters similar to those of earthquakes. This demonstrates that various source parameters of mine tremors have the same physical significance as those of earthquakes in representing the scale of focal rupture and magnitude of regional stress. However, the stress drops of strong mining tremors were orders of magnitude lower than those of earthquakes, indicating that the background stresses of the mining tremors were far smaller than those of earthquakes. This signifies that even relatively small changes in regional stress can potentially trigger the occurrence of mining tremors. We need to pay close attention to factors that can cause regional stress changes during the resource extraction process in mining areas. This provides theoretical support for the monitoring and assessment of the risk associated with strong mine tremors.

Keywords: strong mine tremor, source parameters, response characteristics, genetic algorithm, Brune model

1. Introduction

China produces more coal than any other country on Earth. In 2019, coal consumption accounted for approximately 57.7% of China's energy consumption (Ye et al., 2020). Because of long-term, high-intensity coal mining, large goafs have formed throughout the country (Zhang, 2005; Dong et al., 2020), resulting in frequent mine tremors. For example, the Shandong Digital Seismic Network records as many as 100 mining tremors ($M_L \geq 1.5$) per year. In particular, from 2016–2021, the Shandong Digital Seismic Network recorded 4, 7, 18, 10, 22, and 12 strong mining tremors, with magnitudes above M_L 2.5 in Shandong Province, respectively, generally indicating a gradual increasing trend over time. mining tremors often have high intensities because they have shallow seismic sources, and they often occur in daily production and living areas or near mining and excavation areas (Ju et al., 2019; Qian, 2014; Jiang et al., 2015). Therefore, compared with earthquake events of the same magnitude, mining tremors result in more severe damage and more casualties. For example, on December 25, 2015, an M_L 4.0 mine tremors event in the Wanzhuang gypsum mining area in Pingyi County, Shandong Province, affected three nearby operating gypsum mines and eventually resulted in 13 missing persons and one confirmed death. Therefore, in some mining areas that have been exploited for many years, sudden mining tremors a nonnegligible threat to the local population's productivity and safety. It is worth noting that the vast majority of tremors do not result in accidents. The most impactful on work safety are coal bumps from hard coal mines. Consequently, strengthening research on mining tremors (including coal bump from a hard coal mine) and implementing effective disaster mitigation measures is truly urgent (currently, we are unable to precisely distinguish the subtle differences between tremors, coal bumps, roof collapses, and other types of events solely based on the existing waveform data recorded by the Shandong Digital Seismic Network (This is mainly because the average spacing of 20 kilometers between far-field stations in the Shandong Digital Seismic Network leads to significant attenuation of seismic waves after long-distance propagation, resulting in significant noise on the recordings. Additionally, the heterogeneous geological structures in the Shandong region cause slight signal distortion. Therefore, waveform records lose some characteristic information. It is necessary to integrate near-field stations to accurately distinguish event types).

Mining activities alter the originally stable geological structure, leading to uneven stress in mining areas. Subsequently, the instantaneous instability in local areas releases energy by ejection or downward collapse, which induces violent vibrations and massive damage around the mining areas (Bing et al., 2007; Jiang et al., 2015; Li et al., 2024), also known as mine tremors, including rock bursts that occur during mining and tunneling. When a mine tremor occurs, a portion of the released energy propagates outward from the source as seismic waves, which can be recorded by seismometers (Chen, 2019). Therefore, relevant studies can be conducted based on the waveforms recorded during mine tremors.

Obtaining the characteristic source parameters of a mining tremor directly from its waveform records provides an important basis for studying the rupture process, rupture strength, and source rupture scale of the mining tremor and the stress distribution of the medium around the rupture surface and thus predicting mining area risk (Tang et al., 2011). Source parameters refer to some characteristic quantities or physical processes at the source when an earthquake occurs. Source parameters include corner frequency fc, low-frequency limit Ω_0, seismic moment, source rupture radius, moment magnitude scale M_w, and stress drop. Different specific source parameters have different physical meanings (see section 2.1 of this article for detailed physical definitions). For example, the seismic moment M_0 is a measure of earthquake intensity, reflecting the rupture intensity of an event. The source rupture radius R reflects the size of the source (Li et al., 2023a). Due to their different physical mechanisms, there may be differences in the source parameters. Studies outside China have shown that the stress drops of human activity-induced mining tremors are considerably lower than those of earthquakes (Hough, 2014) and that the stress drops of mine tremors have evident regional characteristics (Lasocki et al., 2008). Many similar studies in China have revealed clear distinction between the source parameters of earthquakes and mining tremors. For example, a comparative analysis of one or several source parameters of earthquakes and mining tremors (Zhang et al., 2005; Nordstrom et al., 2017; Chen, 2019; Yu et al., 2020) has indicated that the corner frequencies of mining tremors are lower than those of earthquakes of similar magnitude (Zhang et al., 2013). The stress drop of a coal bump event (a type of mining tremors) in a mining area is positively correlated with the degree of on-site damage of the rock burst event and can be used as an independent evaluation indicator for the apparent intensity of the seismic source; moreover, a source risk index can be constructed based on the source parameters and used to improve the early warning efficiency in rock burst risk monitoring (Chen, 2019; Xia et al., 2023).

To further deepen the understanding of the source rupture characteristics of mine tremors, this study systematically analyzed the source parameters (corner frequency, low-frequency limit, seismic moment, source rupture radius, moment magnitude, stress drop, etc.) of 39 mine tremors with $M_L \geq 2.5$ recorded by the Shandong Digital Seismic Network from January 2018 to August 2024, summarized their characteristics and the scaling relationships between them, and comparatively analyzed the differences between the source parameters of the mining tremors and those of earthquake events.

2. Method and principles

2.1. Calculation of the corner frequencies and low-frequency limits of the source spectra

The Brune model is widely used in source - parameter inversion for vibration events of different magnitudes and tectonic backgrounds due to its simplicity

and broad applicability (Brune, 1970; Chen et al., 2002). The consistency between its theoretical predictions and observed waveforms has been validated through multiple regional case studies (Nordstrom et al., 2017; Wojtecki et al., 2017). Research demonstrates that the Brune model requires fewer computational resources and is particularly suitable for low-frequency seismic wave-based source parameter inversion (Zhou et al., 2018). Therefore, considering its proven robustness in waveform inversion for $M_L \geq 2.5$ events and its computational efficiency, this study uses the Brune model for source - parameter inversion to balance computational efficiency and inversion accuracy. In this approach, the corner frequency f_c and the low-frequency limit Ω_0 are the bases for calculating the source parameters. According to the Brune model, the theoretical source spectrum $\Omega_0(f)$ satisfies the following equation (Brune, 1970, 1971):

$$\Omega_0(f) = \frac{\Omega_0}{1 + (\frac{f}{f_c})^2}, \tag{1}$$

where f represents the frequency.

Because the amplitude of the P-wave is usually smaller than that of the S-wave and in some special cases, the amplitude of the S-wave can reach approximately 5 times that of the P-wave (Huang, 2003), this article uses the S-wave for numerical calculation. First, the waveform data are preprocessed, mainly including selecting station waveform records with clear seismic phase records and high waveform resolutions (signal-to-noise ratios greater than 1.5). Second, selecting the "S-window" for waveform records, this article selected the time interval from the S-wave to include 90% of its total energy as the "S-window". For the same earthquake, the duration of the "S-window" varies for different seismic stations with different distances from the source. Therefore, to obtain amplitude spectra with the same frequency interval, this study adopted the delay window spectrum technique (Chael, 1987; Huang, 2003) to obtain the displacement spectrum after fast Fourier transform (FFT) transformation.

Usually, $U_{ij}(f)$ represents the seismic displacement spectrum recorded by the digital seismic network:

$$U_{ij}(f) = \left[S_i(f) P_{ij}(f) L'_j(f) + N_j(f) \right] I_j(f) Sur_j, \tag{2}$$

where $S_i(f)$ represents the actual source spectrum of earthquake event i, $P_{ij}(f)$ is the path effect during the propagation of earthquake i to station j, $L'_j(f)$ is the site response of station j, $N_j(f)$ represents the noise near station j, $I_j(f)$ is the instrument response, and Sur_j is the reflection of the seismic wave when it is incident on a free ground surface ($Sur_j = 2$ for surface stations and $Sur_j = 1$ for underground stations). Therefore, the actual source spectrum $S_i(f)$ can be obtained from the seismic displacement spectrum $U_{ij}(f)$ after eliminating the noise term, instrument response, path effect, and site response.

Subsequently, the genetic algorithm was used to fit the source spectrum $S_i(f)$ to obtain the source spectrum parameters: the corner frequency fc and the low-frequency limit Ω_0. The specific steps were as follows: First, using the Brune source model formula (1), a genetic algorithm was used to fit the most suitable combination of Ω_0 and f_c. Theoretically, when the residual was minimized, the average value was closest to the theoretical value, and the obtained Ω_0 and f_c are also most suitable. Therefore, it was necessary to continue fitting until the residual between the theoretical source spectrum and the average source spectrum was minimized. When the residual was minimized, Ω_0 and f_c were obtained. The residual formula is:

$$\varepsilon = \sum_{k=1}^{p} \frac{(teo_k - obs_k)^2}{\sqrt{(teo_k)(obs_k)}}, \tag{3}$$

Teo_k refers to the theoretical source spectrum, and obs_k refers to the average source spectrum.

2.2. Source parameter calculation

Based on f_c and Ω_0, the source parameters of each mine tremor can be calculated using calculation formulas based on the Brune source model (Brune, 1970, 1971).

$$M_0 = \frac{4\pi\rho V_s^3 \Omega_0}{R_{\theta\phi}}, \tag{4}$$

$$R = \frac{2.34 V_s}{2\pi f_c}, \tag{5}$$

$$M_W = \frac{2}{3}\lg M_0 - 6.07, \tag{6}$$

$$\Delta\sigma = \frac{7}{16} \cdot \frac{M_0}{R^3}. \tag{7}$$

Generally, the shear modulus μ of the medium in the source area is 3.0×10^4 MPa, the density ρ of the medium in the study area is 2.7 g cm^{-3}, and the source radiation factor $R_{\theta\varphi}$ is 0.41 (Stork et al., 2004; Yang et al., 2010). For earthquakes, the S-wave propagation velocity $V_S = 3.5$ km s^{-1} in Shandong region was selected (Zhou et al., 2018); for mining tremors, $V_S = 2.1$ km s^{-1} specific to Shandong mining areas was adopted (Chen, 2019; Wu et al., 2023).

The international seismological community uses the Richter scale proposed by Richter to determine the local magnitude M_L of medium and small earthquakes or mining tremors ($M_L < 4.5$). The calculation formula is:

$$M_L = \lg(\frac{A_N + A_E}{2}) + R(\Delta)\,. \tag{8}$$

In the equation, A_N and A_E are the maximum amplitudes of S-waves recorded in the horizontal north–south and east–west directions, respectively, Δ represents the epicentral distance, and $R(\Delta)$ is the measurement error of the short-period seismometer. This work adopted the above method to calculate the magnitude M_L of strong mining tremors.

3. Data

The Shandong Digital Seismic Network consists of 126 stations (including 90 wideband or very wideband seismometers and 36 short-period seismometers). The monitoring instruments can record frequencies from 0.003 Hz to 100 Hz (short - period seismometers: 0.5 Hz–100 Hz), suitable for capturing seismic signals from various vibration and earthquake events. The average interstation distance is 20 km. This setup can ensure that mining tremors and seismic events with $M_L \geq 2.5$ are well recorded by multiple stations, and at the same time, it meets the data requirements for source parameter calculation, namely, clear waveform phase recording and high waveform resolution (signal-to-noise ratio greater than 1.5), and each earthquake can be recorded by at least 3 stations.

From January 2018 to August 2024, the Shandong Digital Seismic Network recorded 69 strong mine tremors with $M_L \geq 2.5$, including an M_L 3.4 (the largest

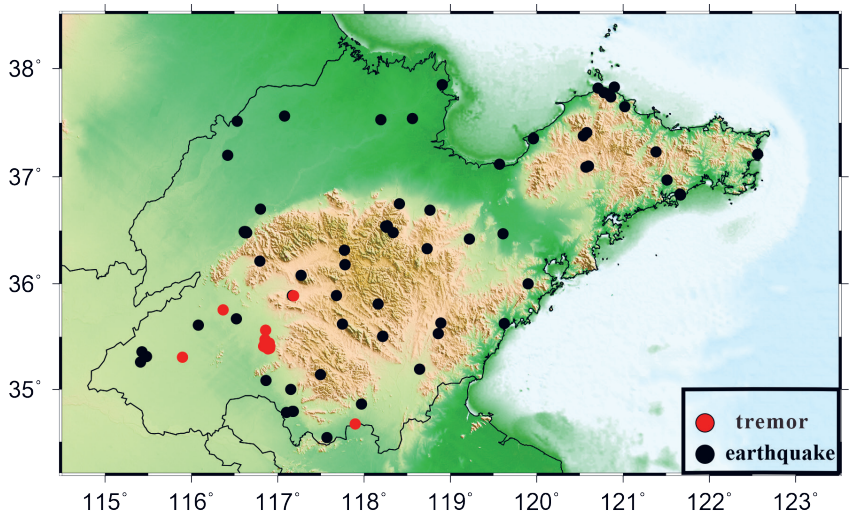

Figure 1. Spatial distribution of $3.4 \geq M_L \geq 2.5$ earthquakes and strong mine tremors recorded by the Shandong Digital Seismic Network from January 2018 to August 2024.

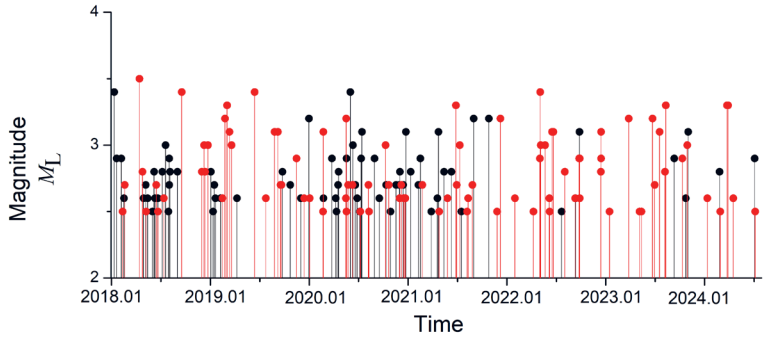

Figure 2. M-T diagram of $3.4 \geq M_L \geq 2.5$ earthquakes and strong mine tremors in the Shandong Digital Seismic Network from January 2018 to August 2024 (Red represents earthquakes, black represents strong mine tremors).

M_L) mine tremor in Zoucheng, Shandong Province, on January 10, 2018. A total of 89 earthquake events with comparable M_L values ($3.4 \geq M_L \geq 2.5$) in the inland area of Shandong Province recorded by the Shandong Digital Seismic Network during the same period (January 2018 to August 2024) were selected for source parameter comparison with the strong mine tremors (Figs. 1 and 2), Notably, Due to the fact that a large number of these strong mine tremors occurred in the same mining area and were highly concentrated spatially, this resulted in the overlapping of red dots (representing mine tremors) in Fig. 1.

4. Calculation results and analysis

To ensure the reliability of the numerical calculations of source parameters, we screened the waveform record data of the events. The specific requirements are as follows: the waveform records of the strong mine tremors recorded by at least three stations with signal-to-noise ratios exceeding 1.5 were used to calculate the source parameters. Finally, 39 (approximately 56.5%) strong mine tremors and 53 (approximately 59.5%) earthquakes in the inland area of Shandong Province were included in this study based on the calculation criteria, and their source parameters were calculated (Tabs. 1 and 2).

4.1. Calculation results of the source parameters of the strong mining tremors

The corner frequency refers to the frequency at the intersection of the low-frequency asymptote and the high-frequency asymptote of the seismic source spectrum, it reflects the distribution characteristics of the high- and low-frequency energy of the seismic wave and the variation characteristics of the attenuation of the seismic wave (Brune, 1970; Savage, 1972). The low-frequency limit refers to the approximate value of the source spectrum at the low frequency. Equations

(1) and (2) show that the corner frequency and the low-frequency limit are obtained simultaneously by determining the minimum residual between the theoretical source spectrum and the average source spectrum of the events after eliminating various influencing factors from the displacement spectrum recorded by the station; thus, the two parameters are not independent of each other. Therefore, only one of these two parameters must be analyzed in most situations. In this study, the corner frequency was selected for analysis. The corner frequencies f_c of the strong mining tremors were between 0.9 and 3 Hz. Compared with earth-quakes of similar magnitudes, the strong mining tremors showed lower corner frequency in the waveform records. This discrepancy primarily arises from differences in their underlying occurrence mechanisms. Earthquakes result from sudden complex fault ruptures that generate abundant high-frequency shear wave radiation, their spectra have a wide range of dominant frequencies, concentrated in 0.5 Hz–15 Hz. In contrast, mining tremors is caused by mining activities, characterized by simpler waveforms dominated by low-frequency surface waves with relatively simple frequency components. Their dominant frequency in the spectrum focus on 0.5 Hz–3 Hz while lacking significant high-frequency content. Furthermore, any weak high-frequency components generated by mining tremors were easily absorbed by the porous medium in which the seismic waves propagated due to the shallow source, simple propagation path, and numerous goafs.

The seismic moment M_0 is a measure of earthquake intensity, reflecting the rupture intensity of an event. For the strong mining tremors in this study, the M_0 values were between 10^{12} and 10^{14} N m, and the moment magnitudes (M_w) were between 2.5 and 3.5 (Tab. 1). The calculated M_w values were slightly larger than the M_L values measured by the Shandong Digital Seismic Network.

The source rupture radius R, which reflects the size of the source, is related to the seismic intensity and the medium structure in the source area (Brune, 1970). An accurate estimate of the source rupture radius of a mining tremor event is an important basis for assessing the impact range of the mining tremor. The R values of the mining tremors in this study were between 300 m and 850 m. The calculation results of this study indicate relatively large source rupture radii for certain events, which deviates from our conventional understanding (generally, the source radius of mining tremors is generally smaller than that of natural earthquakes with the same magnitudes). Combined with on-site investigations of certain mining tremors and the overall research conducted by some researchers on Shandong mining areas, it is shown that the Shandong mining areas predominantly develop within complex geological tectonic settings, with some areas located in tectonic fracture zones, characterized by abundant faults and few folds. Additionally, cataclasite and fault gouge develop near faults or fold zones, making the rock mass highly prone to fragmentation (Wang et al., 2000; Li et al., 2008). Meanwhile, the spatial occurrence of the high-energy events studied in this paper is in goaf areas caused by long-term mining, with

Table 1. Statistical table of calculation results of source parameters for strong mining tremors.

Strong mining tremors	Low-frequency limit (μm×s)	Corner frequency (Hz)	Seismic moment, M_0 (N×m)	Magnitude, M_L	Moment magnitude, M_W	Stress drop (MPa)	Source rupture radius (m)
1	116.03	0.93	2.47×10^{14}	3.4	3.5	0.18	842.52
2	39.94	1.01	8.50×10^{13}	2.9	3.2	0.08	774.70
3	36.63	1.16	7.80×10^{13}	2.9	3.2	0.11	677.38
4	13.37	1.20	2.85×10^{13}	2.6	2.9	0.05	653.68
5	25.88	1.07	5.51×10^{13}	2.6	3.1	0.06	730.77
6	24.93	1.09	5.31×10^{13}	2.7	3.1	0.06	718.32
7	24.47	1.18	5.21×10^{13}	2.6	3.1	0.08	660.86
8	19.54	1.33	4.16×10^{13}	2.6	3.0	0.09	587.95
9	40.93	1.11	8.71×10^{13}	2.8	3.2	0.11	703.71
10	18.74	1.28	3.99×10^{13}	3.0	3.0	0.08	611.21
11	31.56	1.15	6.72×10^{13}	2.8	3.1	0.09	682.21
12	7.83	1.16	1.67×10^{13}	2.5	2.7	0.02	672.72
13	4.48	2.58	9.55×10^{12}	2.7	2.6	0.15	303.11
14	15.43	1.21	3.29×10^{13}	2.6	2.9	0.05	647.34
15	12.86	1.32	2.74×10^{13}	2.6	2.9	0.06	594.66
16	6.16	1.54	1.31×10^{13}	2.7	2.7	0.04	509.48
17	10.18	1.40	2.17×10^{13}	2.6	2.8	0.05	558.30
18	13.32	1.43	2.83×10^{13}	2.9	2.9	0.08	547.95
19	12.16	1.59	2.59×10^{13}	2.6	2.9	0.10	492.59
20	18.18	1.11	3.87×10^{13}	2.5	3.0	0.05	704.01
21	14.28	1.50	3.04×10^{13}	2.8	2.9	0.09	521.25
22	19.16	1.27	4.08×10^{13}	2.9	3.0	0.08	617.88
23	22.88	1.38	4.87×10^{13}	3	3.1	0.12	565.08
24	10.75	1.43	2.29×10^{13}	2.7	2.8	0.06	545.77
25	7.92	1.43	1.69×10^{13}	2.6	2.7	0.05	545.73
26	12.24	1.44	2.60×10^{13}	2.6	2.9	0.07	543.37
27	38.65	0.94	8.23×10^{13}	2.9	3.2	0.06	832.46
28	3.84	1.83	8.17×10^{12}	2.5	2.5	0.05	428.10
29	10.07	1.60	2.14×10^{13}	2.9	2.8	0.08	489.39
30	4.69	1.92	9.97×10^{12}	2.7	2.6	0.07	407.00
31	8.36	1.52	1.78×10^{13}	2.8	2.8	0.06	514.58
32	5.87	1.13	1.25×10^{13}	2.6	2.7	0.02	694.81
33	4.95	1.17	1.05×10^{13}	2.6	2.6	0.02	667.85
34	27.11	1.09	5.77×10^{13}	2.7	3.1	0.07	715.89
35	9.92	1.20	2.11×10^{13}	2.7	2.8	0.03	653.57
36	21.30	1.41	4.53×10^{13}	3.1	3.0	0.12	554.98
37	13.40	1.33	2.85×10^{13}	2.8	2.9	0.06	589.13
38	45.91	1.00	9.77×10^{13}	2.8	3.3	0.09	779.78
39	10.42	1.78	2.22×10^{13}	3.2	2.8	0.11	439.75

Table 2. Statistical table of calculation results of source parameters for earthquake.

Earth-quake	Low-frequency limit (μm×s)	Corner frequency (Hz)	Seismic moment, M_0 (N×m)	Magnitude, M_L	Moment magnitude, M_W	Stress drop (MPa)	Source rupture radius (m)
1	1.92	14.34	6.83×10^{12}	2.7	2.5	3.98	90.91
2	13.36	11.44	4.74×10^{13}	3.5	3	14.04	113.90
3	2.55	11.54	9.06×10^{12}	2.8	2.6	2.75	112.93
4	1.87	15.00	6.63×10^{12}	2.5	2.5	4.42	86.90
5	2.11	13.66	7.47×10^{12}	2.4	2.5	3.76	95.43
6	0.12	4.00	4.08×10^{11}	2.6	1.7	0.01	325.95
7	10.80	8.25	3.83×10^{13}	3.4	3	4.25	158.01
8	2.29	8.91	8.12×10^{12}	2.6	2.5	1.13	146.37
9	0.37	3.39	1.30×10^{12}	2.8	2	0.01	384.42
10	2.95	14.38	1.05×10^{13}	2.9	2.6	6.15	90.64
11	3.34	3.16	1.18×10^{13}	2.6	2.6	0.07	412.47
12	6.23	10.96	2.21×10^{13}	3.2	2.8	5.75	118.92
13	6.55	10.15	2.32×10^{13}	3.1	2.8	4.80	128.38
14	0.42	3.87	1.50×10^{12}	3	2	0.02	336.68
15	5.34	5.26	1.89×10^{13}	2.8	2.8	0.55	247.62
16	12.38	8.47	4.39×10^{13}	3.4	3	5.26	153.99
17	1.59	15.00	5.65×10^{12}	2.6	2.4	3.77	86.90
18	5.60	15.00	1.99×10^{13}	3.1	2.8	13.24	86.90
19	4.57	11.77	1.62×10^{13}	3.1	2.7	5.22	110.80
20	20.08	4.92	7.12×1013	3.7	3.2	1.67	265.13
21	1.99	10.33	7.05×10^{12}	2.6	2.5	1.53	126.23
22	215.32	2.48	7.64×10^{14}	4.4	3.9	2.30	525.75
23	21.66	4.43	7.68×10^{13}	3.7	3.2	1.32	294.53
24	1.78	15.00	6.30×10^{12}	2.5	2.5	4.20	86.90
25	6.65	8.82	2.36×10^{13}	3.1	2.8	3.20	147.79
26	0.28	3.09	9.83×10^{11}	2.6	1.9	0.01	421.73
27	6.89	7.41	2.45×10^{13}	3.2	2.9	1.96	175.94
28	1.09	10.78	3.87×10^{12}	2.5	2.3	0.96	120.87
29	4.07	15.00	1.44×10^{13}	3	2.7	9.62	86.90
30	1.79	7.97	6.33×10^{12}	2.6	2.5	0.63	163.63
31	0.58	2.39	2.06×10^{12}	2.7	2.1	0.01	545.90
32	0.20	4.56	7.18×10^{11}	2.7	1.8	0.01	285.82
33	2.51	8.37	8.92×10^{12}	2.6	2.6	1.03	155.77
34	9.81	7.41	3.48×10^{13}	3.3	3	2.80	175.95
35	2.14	10.06	7.58×10^{12}	2.7	2.5	1.52	129.58
36	5.00	13.34	1.77×10^{13}	3	2.8	8.32	97.70
37	2.64	8.81	9.37×10^{12}	2.5	2.6	1.26	148.04
38	0.19	3.09	6.59×10^{11}	2.6	1.8	0.00	422.15
39	1.54	13.23	5.48×10^{12}	2.7	2.4	2.50	98.57
40	3.25	11.04	1.15×10^{13}	3.2	2.6	3.06	118.11

Table 2. Continued

Earth-quake	Low-frequency limit (μm×s)	Corner frequency (Hz)	Seismic moment, M_0 (N×m)	Magnitude, M_L	Moment magnitude, M_W	Stress drop (MPa)	Source rupture radius (m)
41	4.19	7.27	1.49×10^{13}	2.9	2.7	1.13	179.29
42	10.90	6.54	3.87×10^{13}	3.4	3	2.13	199.43
43	5.63	7.71	2.00×10^{13}	3	2.8	1.80	169.18
44	3.68	9.25	1.31×10^{13}	3	2.7	2.05	140.88
45	3.88	10.00	1.38×10^{13}	3	2.7	2.72	130.39
46	4.38	12.76	1.56×10^{13}	3.1	2.7	6.38	102.19
47	4.97	15.00	1.76×10^{13}	3.1	2.8	11.76	86.90
48	2.16	15.00	7.65×10^{12}	2.5	2.5	5.10	86.90
49	4.87	6.88	1.73×10^{13}	2.7	2.8	1.11	189.47
50	4.73	10.30	1.68×10^{13}	2.7	2.7	3.62	126.59
51	1.99	15.00	7.04×10^{12}	2.5	2.5	4.70	86.90
52	4.76	10.99	1.69×10^{13}	2.6	2.7	4.42	118.65
53	7.98	6.19	2.83×10^{13}	2.7	2.9	1.33	210.52

some events manifesting as roof collapses in these goafs. The occurrence process is often complex, often involving multiple consecutive roof collapses within a short period. However, due to limited monitoring capabilities, these collapses may be recorded as a single event in waveform records due to waveform superposition. These factors may all contribute to the larger-than-expected source radii for some mining tremors. It is worth noting that although mining tremors with the same magnitude generally have smaller source radii than natural earthquakes, their focal depths are typically very shallow. Shallower focal depths of mining tremors are typically a key factor affecting their perceptibility on the surface. These tremors generate stronger seismic waves close to the surface, resulting in greater intensity felt by people and structures.

The instantaneous stress drop is the change in the stress on the fault plane at the moment at which an event occurs and is theoretically defined as the difference between the initial stress (before the event) and the termination stress (after the event). Among events with similar magnitudes, the larger the stress drop is, the higher the source stress of the event. Therefore, the local environmental stress of the source area can be roughly determined based on the magnitude of the stress drop of the event (Pulido et al., 2000; Jiang, 2015). The stress drops of the mining tremors in this study were relatively low, ranging from 0.02 to 0.18 MPa (Tab. 1), indicating that these strong mining tremors essentially occurred under relatively low environmental stress conditions.

4.2. Scaling relationships between the source parameters of mining tremor

Source parameter scaling laws refer to the statistical correlations between different source parameters (corner frequency, low-frequency limit, seismic

moment, rupture radius, moment magnitude, stress drop, etc.). The empirical correlations between source parameters can demonstrate the mutual constraint relationship between source parameters at the level of seismic rupture dynamics (Gao et al., 2012; Chen, 2019).

The correlation between the magnitude and the seismic moment can reflect the state of an underground medium and the state of seismic activity in different regions (Zhou et al., 2018; Li et al., 2023b). Figure 3 shows the relationship between the seismic moment M_0 and the magnitude M_L. M_0 increases semilogarithmically with increasing M_L, namely, $\mathrm{Log}M_0 = 11.185 + 0.842\,M_L$, with a correlation coefficient of 0.60. The correlation coefficient between f_c and the logarithmic value of M_0 is –0.68; that is, the two are inversely correlated (the corner frequency decreases with increasing seismic moment), which is also evidenced by Fig. 4. Many studies have noted a certain linear relationship between the R and M_0 values of an earthquake event (Savage, 1972; Zhou et al., 2020).

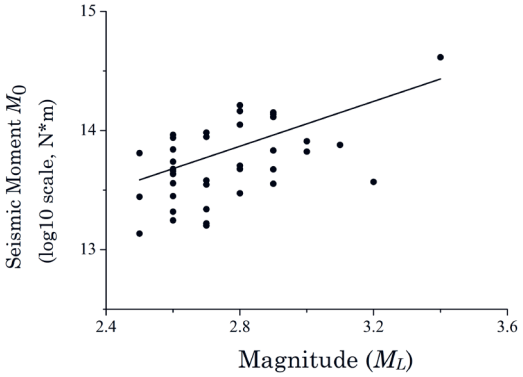

Figure 3. The relationship between seismic moment, M_0 and magnitude, M_L.

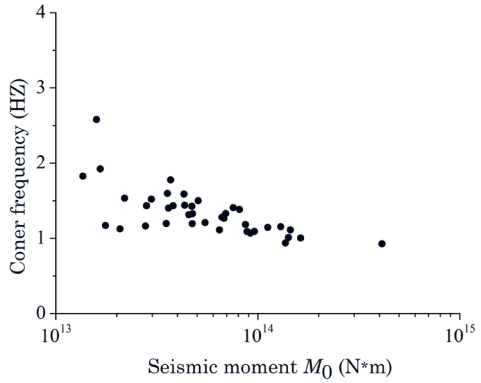

Figure 4. The relationship between corner frequency and seismic moment, M_0.

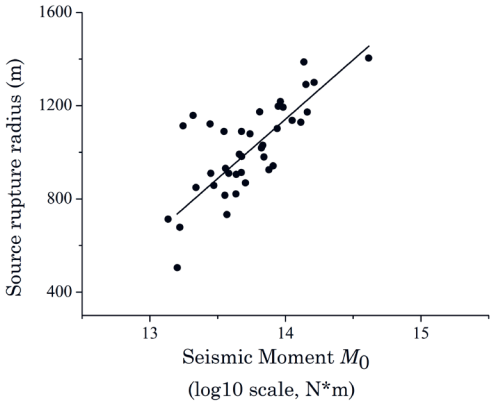

Figure 5. The relationship between rupture radius, R and seismic moment, M_0.

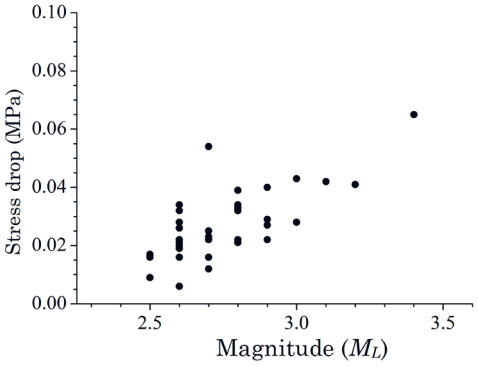

Figure 6. The relationship between stress drop and magnitude M_L.

The linear relationship between R and M_0 of the mining tremors obtained in this study is $\mathrm{Log}M_0 = 11.263 + 0.0037\,R$, with a correlation coefficient of 0.745. Fig. 5 shows that the source rupture radius increases with increasing seismic moment. The stress drop and the magnitude of the mining tremors calculated in this study are significantly correlated, and the stress drop increases with increasing magnitude (Fig. 6). The correlations between the source parameters of the mining tremors are essentially similar to the correlations between the source parameters of earthquakes obtained by other researchers (Allmann et al., 2009; Baltay et al., 2011; Shen et al., 2018; Chen, 2019; Zhou et al., 2020), which indirectly indicates that the source a parameters of mining tremors and earthquakes have the same physical meanings in terms of indicating the rupture strength of events and the magnitude of the regional stress, despite the different physical mechanisms of mining tremors and earthquakes.

4.3. Comparison of the source parameter characteristics of strong mine tremors with those of earthquake

The above results show a correlation between each set of source parameters. Therefore, the characteristics of any source parameter of earthquakes and those of mining tremors can be compared to indirectly comparatively analyze the characteristics of other parameters between the two types of events. In addition, the stress drop of an event represents the environmental stress level in the source region of the event, which is of great importance for analyzing the regional seismic activity trend. Therefore, the stress drop was selected to compare the characteristics of the differences between the source parameters of earthquakes and mining tremors. Figure 7 shows the stress drops of natural earthquakes and mining tremors. This figure indicates that the stress drop of an earthquake is substantially (by orders of magnitude) greater than that of a mining tremor, Magnitude depends on the amount of energy released, and since mining tremors are typically associated with localized, man-made activities, they usually have lower magnitudes compared to earthquakes under similar environmental stresses.

The mining tremors and earthquakes show substantial differences in source parameter characteristics for the following two reasons. First, the two types of events are sliding events with completely different physical mechanisms. Strong mine tremors are triggered mainly by the change in stress in the mining area due to mining activity-induced changes in the originally stable geological structure (Jiang et al., 2015). E arthquakes refer to rupture dislocations of the Earth's deep crust under plate tectonic-induced stresses or the expansion and instability of the original faults; they occur when the stress-induced deformation of deep rock exceeds a certain threshold. When the two types of events occur, the respective background environmental stress states are different because of their different physical triggering mechanisms. Second, the mining areas where mining tremors occur often have large goafs under the rock strata due to persistent mining. Hence, a small stress can cause rock subsidence, resulting in strong mining tremors. In other words, mining tremors can occur in low-stress environments.

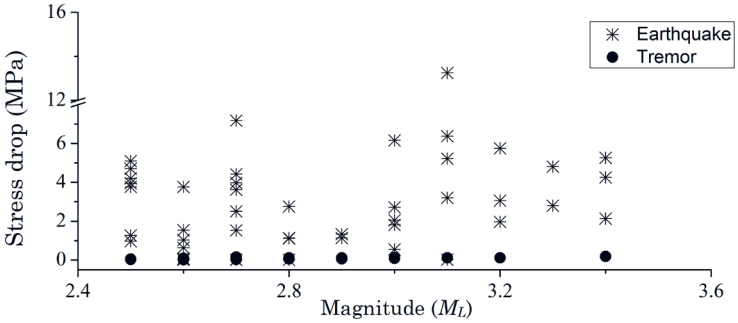

Figure 7. Distribution of stress drops for earthquakes and mining tremors.

5. Discussion and conclusion

In this study, we systematically investigated the source parameter characteristics and their scaling relationships for 39 strong mining tremors of magnitudes 2.5–3.4. The calculated corner frequencies f_c, seismic moments M_0, moment magnitudes M_W, and stress drops of the strong mine tremors with magnitudes of 2.5–3.4 were 0.9–2.6 Hz, 10^{12}–10^{14} N m, 2.5–3.5, and 0.02–0.18 MPa, respectively. The results show that the strong mine tremors had a low proportion of high-frequency components in the waveform records, slightly smaller M_L values than M_w values, and relatively low stress drops, which reflects that a mining tremor generates a much lower background environmental stress.

The source parameters of the strong mine tremors were correlated. The seismic moment increased with increasing M_L, and the correlation coefficient and fitted linear correlation between the two parameters were 0.60 and $\mathrm{Log}M_0 = 11.185 + 0.842\,M_L$, respectively. The corner frequency f_c and the seismic moment were inversely correlated, *i.e.*, the corner frequency decreased with increasing seismic moment. The source rupture radius of a mining tremor increased with increasing seismic moment, and the correlation coefficient and fitted linear relationship between the two parameters were 0.745 and $\mathrm{Log}M_0 = 11.263 + 0.0037\,R$, respectively. The stress drop of a mining tremor increased with increasing magnitude. The correlations between the source parameters of the mining tremors obtained in this study were essentially similar to those of the source parameters of earthquakes reported in related studies, which indirectly indicates that the source parameters of mining tremors and earthquakes have the same physical meanings in terms of indicating the rupture strength of the events and the magnitude of the regional stress, despite the different physical mechanisms of mining tremors and earthquakes.

Since the source parameters of the strong mine tremors were correlated and each correlation was similar to that of earthquakes, the stress drop, which can represent the environmental stress state of the source area of an event, was selected to compare the source parameter characteristics of earthquakes and mining tremors. The results show that the stress drops of the mining tremors were orders of magnitude lower than those of earthquakes, which reflects that a mining tremor generates a much lower background environmental stress than an earthquake. The mining tremors and earthquakes showed considerable differences in source parameter characteristics mainly due to their different specific physical mechanisms and the occurrence of mining tremors in the goofs.

In summary, the source parameters of strong mine tremors and earthquakes have both similarities and unique characteristics, which indicates that strong mine tremors and earthquakes have differences in their physical mechanisms. In the future, we must monitor and evaluate mining tremors by learning from the theories and analysis methods of earthquakes while considering their differences from earthquakes.

Funding: This study is funded by the National Natural Science Foundation of China (42474189) and Science and Technology Innovation Team of Shandong Earthquake Agency – Monitoring of unnatural earthquakes and research on activity mechanism.

Informed Consent Statement: Not applicable.

Data Availability Statement: The waveform recordings of the earthquake and mining tremors used to support the findings of this study were supplied by the Earthquake Agency of Shandong Seismological Bureau under license and thus cannot be made freely available. Requests for access to these data should be made to Shaohui Zhou by emailing 674891062@qq.com.

Conflicts of Interest: The authors declare no conflict of interest.

References

Allmann, B. P. and Shearer, P. M. (2009): Global variations of stress drop for moderate to large earthquakes, *J. Geophys. Res.*, **114**(B1), 310–332, https://doi.org/10.1029/2008JB005821.

Baltay, A., Ide, S., Prieto, G. and Beroza, G. (2011): Variability in earthquake stress drop and apparent stress, *Geophys. Res. Lett.*, **38**(6), 122–133, https://doi.org/10.1029/2011GL046698.

Bing, S. D. and Yi, S. P. (2007): Research on the method and application of microseismic positioning in mines, *J. Min. Strata Control Eng.*, **12**(5), 1–4.

Brune, J. N. (1970): Tectonic stress and the spectra of seismic waves from earthquakes, *J. Geophys. Res.*, **75**, 4997–5009, https://doi.org/10.1029/JB075i026p04997.

Brune, J. N. (1971): Correction [to "Tectonic Stress and the Spectra of Seismic Shear Waves from Earthquakes"], *J. Geophys. Res.*, **76**(20), 5002, https://doi.org/10.1029/JB076i020p05002.

Chael, E. P. (1987): Spectral scaling of earthquakes in the Miramichi region of New Brunswick, *B. Seismol. Soc. Am.*, **77**(2), 347–365, https://doi.org/10.1785/BSSA0770020347.

Chen, D. (2019): Study on the Source Parameters and Rupture Mechanism of Micro-earthquakes in Coal Mine. PhD Thesis, China University of Mining and Technology, Xuzhou in China, 43–99 pp, https://cdmd.cnki.com.cn/Article/CDMD-10290-1019603740.htm.

Chen, F. (2019): Failure Mechanism of Mining Induced Tremorand Response Law of Its Source Mechanics Parameters. Master's Thesis, China University of Mining and Technology, Xuzhou in China, 72–81 pp, https://cdmd.cnki.com.cn/article/cdmd-10290-1019854091.htm.

Chen, S. and Atkinson, G. M. (2002): Global comparison of earthquake source spectra, *B. Seismol. Soc. Am.*, **92**, 885–895, https://doi.org/10.1785/0120010152.

Dong, C. L., Wang, Z. J., Zhang, N., Ding, X. W. and Guo, L. Q. (2020): Mechanism and cause of two collapsed earthquakes in Daixian and Fanshi, Northeast of Shanxi Province, *Earthquake Research in China*, **36**(1), 80–90.

Gao, H. Y., Schmidt, D. A. and Weldon, R. J. II. (2012): Scaling relationships of source parameters for slip events, *B. Seismol. Soc. Am.*, **102**(1), 352–360, https://doi.org/10.1785/0120110096.

Huang, Y. L., Zheng, S. H., Liu, J., Zhao, X. Q. and Kang, Y. (2003): Seismic ground motion attenuation and site response in Guangdong Province, *Chinese J. Geophys.*, **46**(1), 54–61.

Hough, S. E. (2014): Shaking from injection-induced earthquakes in the Central and Eastern United States, *B. Seismol. Soc. Am.*, **104**(5), 2619–2626, https://doi.org/10.1785/0120140099.

Jiang, H. K., Yang, M. L., Fu, H., Gao, G. Y. and Tian, Q. J. (2015): Reference guide for postearthquake trend determination. Seismological Press, Beijing in China, 71–86 pp.

Jiang, Y. D. and Zhao, Y. X. (2015): State of the art: Investigation on mechanism, forecast, and control of coal bumps in China, *Chinese J. Rock Mechanics and Engineering*, **34**(11), 2188–2204.

Lasocki, S. and Orlecka-Sikora, B. (2008): Seismic hazard assessment under complex source size distribution of mining-induced seismicity, *Tectonophysics*, **456**(1/2), 28–37, https://doi.org/10.1016/j.tecto.2006.08.013.

Li, J., Jiang, H. and Wang, Q. (2023): Crustal attenuation structure of the Tianshan tectonic belt and its spatiotemporal variations, *Front. Earth Sci.*, **11**, 1094151, https://doi.org/10.3389/feart.2023.1094151.

Li, J., Gao, Y. and Zhou, S. (2023): Upper crust anisotropy of the 2020 Jiashi M_S 6.4 earthquake, *Front. Earth Sci.*, **11**, 1160676, https://doi.org/10.3389/feart.2023.1160676.

Li, T. B., Xu, W. H., Ma, C. C., Zhang, H., Zhang, Y. X. and Dai, K. K., (2024): Research on tunnel micro-seismic monitoring and rock burst warning technology and system based on deep learning, *Chinese J. Rock Mechanics and Engineering*, **43**(05), 1041–1063, https://doi.org/10.13722/j.cnki.jrme.2023.0433.

Li, N., Liu, J., Liu, S. L. and Tian, L. Q. (2008): Structural Characteristics of Yangzhuang Coal Fault and Its Influences to the Production in Yanzhou Coal Mine of Shandong Province, *Shandong Land and Resources*, **24**(7), 44–46. http://www.sdgt1985.com/sdgtzy/article/abstract/20080721?st=article_issue.

Nordstrom, E., Dineva, S. and Nordlund, E. (2017): Source parameters of seismic events potentially associated with damage in block 33/34 of the Kiirunavaara mine (Sweden), *Acta Geophysica*, **65**(6), 1229–1242, https://doi.org/10.1007/s11600-017-0066-1.

Pulido, N. and Irikura, K. (2000): Estimation of dynamic rupture parameters from the radiated seismic energy and apparent stress, *Geophys. Res. Lett.*, **27**(23), 3945–3948, https://doi.org/10.1029/2000GL011658.

Qian, Q. H. (2014): Definition, mechanism, classification and quantitative forecast model for rockburst and pressure bump, *Rock Soil Mech.*, **35**(1), 1–6, https://doi.org/10.16285/j.rsm.2014.01.028.

Savage, J. C. (1972): Relation of corner frequency to fault dimensions, *J. Geophys. Res.*, **77**(77), 3788–3795, https://doi.org/10.1029/JB077i020p03788.

Stork, A. L. and Ito, H. (2004): Source parameter scaling for small earthquakes observed at the western Nagano 800-m-deep borehole, central Japan, *B. Seismol. Soc. Am.*, **94**(5), 1781–1794, https://doi.org/10.1785/012002214.

Wang, B. S. and Wang, X.E. (2000): Characteristics of extensional structures in western shandong and their influence on coal mine production, *Coal Geol. Explor.*, 28(3), 20–24, https://doi.org/10.3969/j.issn.1001-1986.2000.03.007.

Wu, K. B., Zou, J. P., Jiao, Y. Y. and Hu, X. Y. (2023): Analysis of source parameters and source mechanism of strong tremors in deep coal mines, *Chinese J. Rock Mech. Eng.*, **42**(10), 2540–2551.

Shen, X. L., Wei,G. C.,Ding, W. Q. and Dai, M. (2018): Study on seismic source parameters in Hubei Region, *Earthq. Res. China*, **34**(4). 781–787.

Tang, L. Z., Ling, H. W. and Jun, Z. (2011): Earthquake stress drop and deformation in large-scale mining and prediction of regional dangerous earthquakes, *Chinese J. Rock Mech. Eng.*, **30**(6), 1168–1178.

Xia, C. Y., Wang, L. and Wang, Y. (2023): Research on characteristics of source parameters of Kangping mine tremors based on Brune model, *J. Disaster Prevention and Mitigation*, **39**(4), 43–47.

Wojtecki, L., Mendecki, M. J. and Zuberek, W. M. (2017): Determination of destress blasting effectiveness usingmining tremor parameters, *Rock Mech. Rock Eng.*, **50**(12), 3233–3244, https://doi.org/10.1007/s00603-017-1297-9.

Yu, G. C., Yao, Y. S., Zhang, L. F., Wang, Q. L. and Wu, H. B. (2020): Study on the genesis of M_S≥5 earthquake swarm in Songyuan area, Jilin Province, China in 2013, *Journal of Geodesy and Geodynamics*, **40**(5), 534–539 (in Chinese).

Yaodong, J. and Zhao, Y. X. (2015): State of the art: Investigation on mechanism, forecast and control of coal bumps in China, *Chinese J. Rock Mech. Eng.*, **34**(11), 2188–2204.

Yang, J. Q., Yang, Z. S., Liu, L. F., Su, Y. J. and Zhang, S. (2010): Study on the source parameters of the Yingjiang M_S5.9 earthquake sequence in 2008, *J. Seismol. Res.*, **33**(4), 308–312+376.

Ye, C., Wang, J. and Chen, Y. (2020): China energy development report. Social Sciences Academic Press (China), Beijing in China, 21 pp.

Zhang, L. F., Yao, Y. S., Li, J. G., Wu, H. B. (2013): Corner frequency characteristic of tectonic earthquakes and collapsed ones in threegorges region, *J. Geodesy Geodyn.*, **33**(2), 27–30, https://doi.org/10.14075/j.jgg.2013.02.032.

Zhang, P., Jiang, X. Q., Miao C. L., Zhou, X. R. (2005): *The differences of wave spectrum among explosion, mine tremor and earthquake, Seismological and Geomagnetic Observation and Research*, **26**(3), 24–34.

Zhang, Y. Z. (2005): Analysis of ground collapse control factors and surface stability in Xitieshan Mine. Master's Thesis, Kunming University of Science and Technology, Kunming in china, 6pp. https://d.wanfangdata.com.cn/thesis/Y831682.

Zhou, S. H., Jiang, H. K., Qu, J. H. and Li, J. (2018): A review on research of stress drop, *Earthquake Research in China*, **34**(4), 591–605.

Zhou, S. H., Jiang, H. K., Qu, J. H., Zheng, X., Guo, Z., Li, Y. J. and Zhang, Z. H. (2020): Source parameters of the 2014 *M* 6.6 earthquake sequence in Jinggu, Yunnan, China, *Earthq. Eng. J.*, **42**(6), 1565–1572, https://doi.org/10.3969/j.issn.1000-0844.2020.06.1565.

SAŽETAK

Istraživanje svojstava odziva parametara izvora pri jakim rudarskim podrhtavanjima

Shaohui Zhou, Junhao Qu, Shuang Wu i Yu Wang

Rudarska podrhtavanja značajan su čimbenik koji doprinosi nesrećama u rudarskim područjima, a proučavanje karakteristika izvora pri njihovom nastanku od ključne je važnosti za bolje razumijevanje nastanka povezanih katastrofa. Ovaj rad detaljno analizira 39 jakih rudarskih podrhtavanja u rudarskim područjima u provinciji Shandong u Kini, koristeći kombinaciju numeričkih simulacija i teorijskih analiza. Prvo se na seizmograme jakih rudarskih podrhtavanja primjenjuje brza Fourierova transformacija (FFT). Zatim se iz zapisa uklanjaju šum, odziv instrumenta, učinak medija u kojem se valovi šire, kao i odziv lokalnog svojstva tla mjernih postaja. Na temelju Bruneovog modela izvora, primijenjen je genetski algoritam za prilagodbu i dobivanje parametara izvora. Analiziraju se karakteristike odziva parametara izbora jakih rudarskih podrhtavanja te se određuje razmjer žarišne plohe loma i karakteristike oslobađanja regionalne napetosti. Rezultati su pokazali da su izračunate granične frekvencije, seizmički momenti, momentne magnitude i pad napetosti prilikom jakih rudarskih podrhtavanja bili u rasponima od 0,9–2,6 Hz, 10^{12}–10^{14} N m, 2,5–3,5 i 0,02–0,18 MPa. Rezultati su također pokazaju sličnost između međukorelacije rudarskih podrhtavanja i potresa, ukazujući da različiti parametri izvora rudarskih podrhtavanja imaju isto fizikalno značenje kao i kod potresa u prikazivanju razmjera žarišne plohe loma i razine regionalne napetosti. Međutim, pad napetosti kod jakih rudarskih podrhtavanja za redove veličine manje nego kod potresa, što ukazuje da su pozadinska naprezanja kod rudarskih podrhtavanja znatno manja nego kod potresa. To znači da čak i relativno male promjene u iznosu regionalne napetosti mogu potencijalno izazvati rudarska podrhtavanja. Stoga je potrebno posvetiti posebnu pažnju čimbenicima koji mogu uzrokovati promjene u regionalnoj napetosti tijekom procesa eksploatacije resursa u rudarskim područjima.

Ključne riječi: snažno rudarsko podrhtavanje, parametri izvora, karakteristike odziva, genetski algoritam, Bruneov model

Corresponding author's address: Junhao Qu, 2066 Gangxi Road, Ganggou Street, Licheng District, Jinan City, Shandong Province, China; e-mail: gisquh@126.com

This work is licensed under a Creative Commons Attribution-NonCommercial 4.0 International License.